DARPA CRANE Circulation Control using Arrays of Discrete Fluidic Actuator Jets

Bojan Vukasinovic [1], Robert B. Funk [2], and Ari Glezer[3]
[1,3]*Woodruff School of Mechanical Engineering,*
Georgia Institute of Technology, Atlanta, GA 30332-0405
[2]*Georgia Tech Research Institute ATAS, Smyrna, GA 30080*

Abstract

Controlled modification of an airfoil's circulation to effect significant lift increments by using fluidic-based actuation near its trailing edge was demonstrated in a large body of earlier investigations. In these works, the circulation has been commonly varied by exploiting the Coanda effect over a bluff trailing edge or the airfoil's flap using a nominally 2-D tangential wall jet. More recently, high-lift performance over flaps has been demonstrated using a spanwise array of discrete, 3-D wall jets effected by fluidic oscillators with significant savings in actuation mass flow rates. The present investigation focuses on the utilization of such discrete Coanda actuation using a trailing edge array of fluidic oscillating wall jets integrated into the rounded trailing edge of a 2-D supercritical airfoil model, and their aerodynamic performance over a range of spanwise distributions, and scaling is compared with corresponding 2-D conventional wall jets at low angles of attack ($-5° < \alpha < 5°$) and $Re = 4.7 – 6.1\times10^5$. The investigation compares the effects of the 2- and 3-D Coanda circulation control actuation over a central spanwise segment of the airfoil with actuation over its entire span. The present investigations show that segmented circulation control leads to lift increments of up to $\Delta C_L \approx 2$ at $C_\mu \approx 0.1$. At given actuation mass flow ($C_q = 0.6\%$) the 3-D Coanda wall jets effect about 60% higher lift increment relative to the 2-D jet (1.2 vs. 0.75) and 100% higher C_μ (0.07 vs. 0.035) with significantly lower induced drag penalty $\Delta C_{D,cir}$ (0.04 vs. 0.07). Finally, it is shown that when C_μ is scaled by the actuation area ratio and its spanwise duty cycle, the variations of ΔC_L and ΔC_D with the scaled C_μ exhibit remarkable collapse for all 3-D jet arrays tested. The collapsed data suggest that the induced drag over the present Coanda surface has a local maximum and thereafter diminishes even though the lift increment continues to increase.

I. Background

High-lift enhancement on aircraft wings by modifying the flow near the wings' trailing edges using integrated 2-D high-speed wall-bounded or free jets issuing either tangent to a flap or at the trailing edge of an airfoil at some fixed angle was investigated in the 1950s (e.g., Davidson 1956, Williams et al. 1961). The modification of the embedding flow over the airfoil by the presence of the jet (or 'jet flap' as it was called) led lift increase that was larger than the vertical component of the jet thrust. More advanced aerodynamic circulation control evolved from the jet flap approach by exploiting the Coanda effect associated with a 2-D wall jet issuing over a curved trailing edge of an airfoil or a curved surface of a flap (e.g., Englar 1996, 2000, 2005). The presence of the jet

---

[1] Research Engineer, AIAA Member.
[2] Research Engineer, AIAA Associate Fellow.
[3] Professor, AIAA Fellow.

delays aft flow separation over the curved surface where the extent of the attached flow increases with jet momentum coefficient and the attachment over the Coanda surface leads to partial vectoring of the flow over the surface that, depending on the jet momentum, can reach complete turning that opposes the oncoming flow on the airfoil's other side. The interaction of the actuation or control jet with the cross flow alters the flow and the stagnation point at the trailing edge.

The Coanda effect associated with the evolution of an isolated 2-D turbulent wall jet issuing tangentially over a curved surface in the absence of a cross flow was first analyzed in a seminal paper by Newman (1961) who characterized the deflection of the jet along the surface of a cylinder including changes in distribution of its cross-stream velocity, surface pressure and separation. In a related experimental investigation, Neuendorf and Wygnanski (1999) characterized the evolution of a wall jet over a circular cylinder and identified the conditions under which separation occurs. In a follow-on paper, Neuendorf et al. (2004) characterized the streamwise vortices within the turbulent wall jet that are formed on the convex surface as a result of a centrifugal instability and identified the presence of counter-rotating vortex pairs that migrate along the cylinder axis and were believed to affect separation from the surface. The Coanda effect on the surface of a cylinder becomes more prominent in the presence of a cross flow when the streamwise extent of flow attachment over one side of the cylinder is increased resulting in flow asymmetry over the cylinder and in a large force (normal to the cross-flow direction) that is accompanied by change in the azimuthal position of the front and rear stagnation points and circumferential circulation. For example, Lockwood (1960) reported that a wall jet having a momentum coefficient $C_\mu = 0.15$ results in a normal force coefficient $C_N = 3$ and showed that larger forces can be realized using multiple tangential jets at successive azimuthal positions along the circumference of the cylinder. In a later work, Dunham (1968) developed a model based on boundary layer theory and potential flow formulation to estimate the location of flow separation on a cylinder for a given free stream Reynolds number and a given wall jet slot width and azimuthal orientation, and its momentum coefficient, which was subsequently used to estimate the resulting normal force with good agreement with prior experiments.

The Coanda effect was adapted by a number of investigators for modifying the circulation of conventional airfoils to effect high-lift and enhanced STOL performance, most notably in the body of works by Englar and his co-investigators (e.g., 1996, 2000, 2005, 2013). For example, Englar and Blaylock (2013) demonstrated that a 2-D jet blowing over a circulation control wing (NASA 17%-thick supercritical airfoil) with a rounded trailing edge ($r = 0.036c$) can lead to lift coefficients of up to 8-9 at low angles of attack that far exceeds the lift capability of airfoils with conventional multiple-slotted flaps. Englar and his co-authors noted that circulation control, as it came to be known, is effective over a broad range of angles of attack (augmented with leading edge flow control post stall), can enable significant reduction in the dimensions of conventional control surfaces, and attains high lift to actuation thrust ratio (although lift augmentation can require high actuation momentum coefficient). Englar et al. (1981) reported the use of circulation control for augmenting the STOL capabilities of an A-6 flight demonstrator and reported that their wind tunnel and flight test investigations demonstrated two-fold increase in lifting capabilities. In a later investigation, Loth and Boasson (1984) reported optimization of an internal wall jet ejector that can substantially improve the aerodynamic performance characteristics of the high lift airfoil.

Unsteady aerodynamic Coanda effects realized by a time-periodic 2-D wall jet over a circular cylinder ($Re = 1.9 \cdot 10^5$) were investigated by Ghee and Leishman (1992), who reported that for reduced frequencies $k \leq 0.2$, the induced time-averaged normal aerodynamic load could be increased by up to 50% compared to steady actuation at the same momentum coefficient. In a later study, Jones and Englar (2003) used pulsed blowing of the 2-D actuation wall jet through a full-span slot on a rounded and a dual-radius NASA supercritical airfoil and reported that the actuation mass flow rate required for a given lift coefficient was reduced by more than 50%. Also, for a given C_μ, a higher C_L was attained for the unsteady actuation (at $C_\mu = 0.015$, C_L was increased from 2.7 to 3). More recently, DeSalvo et al. (2016, 2020) investigated high lift enhancement by the Coanda effect of a spanwise array of fluidically-oscillating wall jets on the curved surfaces of a simple flaps and demonstrated an increase in lift of about $\Delta C_L = 1.4$.

In the present investigations, the earlier high lift works of DeSalvo et al. (2016, 2020) were extended to utilize discrete spanwise arrays of fluidically oscillating wall jets over a range of spanwise distribution and scaling for circulation control over a 2-D airfoil having a circular trailing edge Coanda surface with emphasis on STOL performance at low angles of attack ($-5° < \alpha < 5°$). The primary objective is to exploit the spanwise-segmented three-dimensional unsteady Coanda effect to improve circulation enhancement compared to a conventional single 2-D wall jet at the same operating conditions with significant savings in actuation mass flow rates. The investigation compares the effects of the 2- and 3-D Coanda actuation over a central spanwise segment (1/3 span) of the airfoil with actuation over its entire span. Preliminary results of this work were presented by Vukasinovic et al (2021).

II. Experimental Setup and Procedures

The present wind tunnel experiments were conducted using a modified version of the 2-D NASA 17%-thick supercritical airfoil used by Englar et al. (1994) having a chord c = 212mm, thickness t = 23 mm and span L = 762 mm (Figure 1a). In the present configuration, the model did not have a flap and was configured with an interchangeable 2-D quarter-cylinder trailing edge Coanda surface with a circular cross section having a radius R = 12.5 mm that was designed for integration of either a spanwise-uniform 2-D wall jet (Figure 1a) or an array of spanwise oscillating jets (Figure 1b). The 2- and 3-D wall jets were driven from an internal spanwise compressed air plenum that is connected to an external pressure source. While the 2-D jet is engendered using an internal contraction formed by an extension of the quarter cylinder and the top cover of the plenum (on the suction side of the airfoil), the fluidically oscillating wall jets were constructed out of a monolithic stereo lithographed (SLA) module that is inserted into the plenum under its top surface and their orifices form a step above the surface of the quarter cylinder. This modular approach enables interchangeability and testing of different 2- and 3-D actuation configurations. In the present investigations the aerodynamic performance of circulation control actuation over a central spanwise segment (1/3 span) of the airfoil was compared with similar actuation over the entire

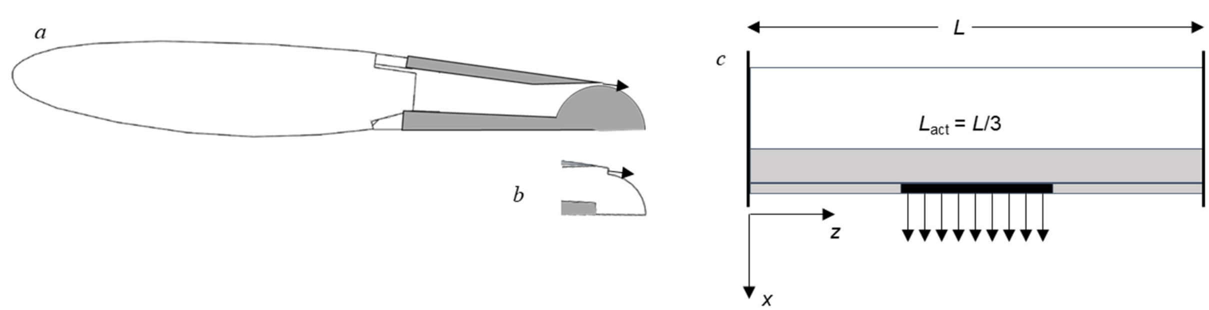

Figure 1. *a) The airfoil model with conventional 2-D wall jet circulation control, b) The corresponding 3-D wall jet module, and c) Schematic planform view of the airfoil showing the active actuation centered about mid-span.*

span (Figure 1c). When actuation was applied at the center span segment, the outboard sections were configured with the same trailing edge geometry but with inactive jets.

The airfoil model was mounted vertically in a subsonic closed-return tunnel (e.g., Englar et al., 1994) having a test section measuring 76.2 x 86.3 cm in which a tangential wall blowing system on the top and bottom walls provided combined calibrated blowing to compensate for interactions between the trailing edge actuation jets and tunnel wall boundary layers (e.g., Englar et al., 1994). The aerodynamic loads were measured using an integrated force balance mounted on the outside of the tunnel's floor and the model spans $L = 762$ mm from tunnel floor to within 2 mm of the test section ceiling using a thin endplate, and is mounted on a 30 cm base plate that is attached to the floor balance. The aerodynamic loads on the baseline 2-D airfoil in the absence of actuation were characterized over a range of the angles of attack (α) and the variations of the lift and drag with α over the range $-10^{\circ} < \alpha < 18^{\circ}$ are shown for reference in Figure 2 and indicate that the onset of stall occurs at $\alpha \approx 13°$. The drag is nearly invariant $-5^{\circ} < \alpha < 0^{\circ}$ ($C_D \approx 0.047$) and thereafter increases monotonically (at 10°, $C_D \approx 0.074$). As noted above, in the present investigations the primary interest is in STOL performance at low angles of attack and so attention is restricted to $-5° < \alpha < 5°$.

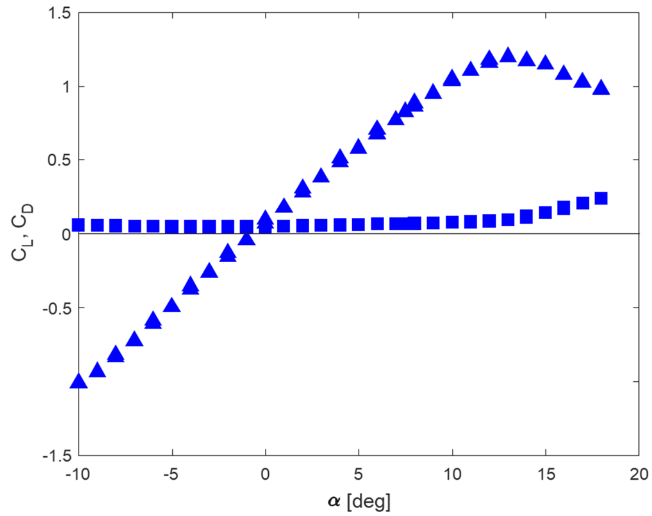

Figure 2. Variation of the lift (▲) and drag (■) with angle of attack for the baseline airfoil model with inactive flow control modules, $Re = 4.7 \cdot 10^5$.

III. Coanda Flow Control using Discrete Actuation

The 2- and 3-D actuation wall jets were driven by the laboratory compressor system and the actuation mass flow rate $\dot{m}_{jet}$ was monitored using standard flow meters. The actuation performance was characterized using the momentum coefficient $C_\mu = T/(q \cdot c \cdot L_{act})$ and mass flow rate coefficient $C_q = \dot{m}_{jet}/(\rho_o \cdot U_o \cdot c \cdot L_{act})$ where T is the actuation thrust, q is the tunnel's dynamic pressure and L_{act} is the span of the airfoil's active actuation segment (in the present investigations, $L_{act} = L$ and $L/3$). The thrust or Coanda force of the 2-D wall jets issuing upstream of the circular (quarter cylinder) trailing edge (Figure 1) was measured *in situ* using the wind tunnel's 6-component force balance in the absence of cross flow along with the corresponding actuation mass flow rate $\dot{m}_{jet}$.

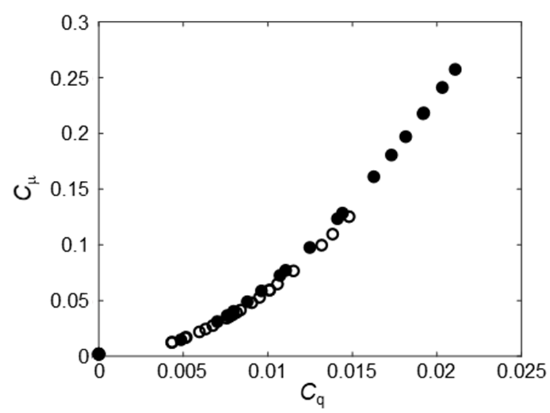

Figure 3. Variation of the C_μ with C_q (at $U_o = 35$ m/s) in the absence of cross flow for the 2-D jets h_1 (○) and h_2 (●).

Two 2-D Coanda wall jets having orifice heights $h_1 = 0.5$ mm and $h_2 = 0.82h_1$ that are referred to below as configurations C2D-1 and -2 were tested. The variations of C_μ with C_q for these 2-D configurations were assessed for a nominal tunnel speed $U_o = 35$ m/s and are shown in Figure 3. As expected, $C_\mu \sim C_q^2$ and the scaled distributions for C2D-1 and -2 exhibit a reasonably similar overlap for $C_q < 0.015$.

The performance of spanwise arrays of discrete fluidically oscillating wall jets mounted upstream of a similar circular (quarter cylinder) surface was first explored in benchtop investigations using monolithic modules fabricated using SLA. Each module included an array of equally spaced actuation jets that was attached to a pressurized plenum in a test cell equipped with a 6-component balance and the actuation air flow rate was measured using a thermal mass flow sensor. The performance of the jet arrays was assessed by measuring the two components of the developed force in the cross stream and streamwise directions T_x and T_y, respectively and was directly compared with 2-D wall jets having the same spanwise extent. The selection of the characteristic dimensions of the exit orifices of the fluidic actuators was guided by the ratio of the height of the 2-D continuous jet to Coanda surface radius h/R that yielded good aerodynamic performance in the earlier investigations of Englar et al. (1994, 2000, 2005). The Coanda effect was characterized by considering the total force and the angle between T_y and T_x that measures the turning of the wall jet over the Coanda surface in the absence of a cross flow. The side force T_z is a measure of the spanwise symmetry of the actuators and was nearly zero in the present measurements.

While multiple combinations of jet arrays and Coanda surfaces were bench tested, two specific configurations of 3-D wall jet arrays were selected for assessment of their aerodynamic performance on the airfoil model. These configurations were compared with the corresponding 2-D jet in terms of variation of the jet-induced Coanda forces with actuation mass flow rate. Figure 4 shows the performance of two 3-D configurations that are referred to as C3D-1 [10 jets, centerlines spacing 8.75 mm apart, and 1.5 x 1 mm (spanwise $AR = 0.66$) orifices] and C3D-2 [5 jets, centerlines spacing 18 mm apart, and 1 x 3 mm (spanwise $AR = 3$) orifices] in a single bench-test control module that spans $L/6$. The total active orifice areas of the arrays C3D-1 and -2 relative to the C2D-1 jet (A_1) are $0.34A_1$ and $0.29A_1$ respectively. The variations with normalized actuation mass flow rate $\dot{m}_j/\dot{m}_{j,o}$ of the ratio of the measured forces developed on the same Coanda surface

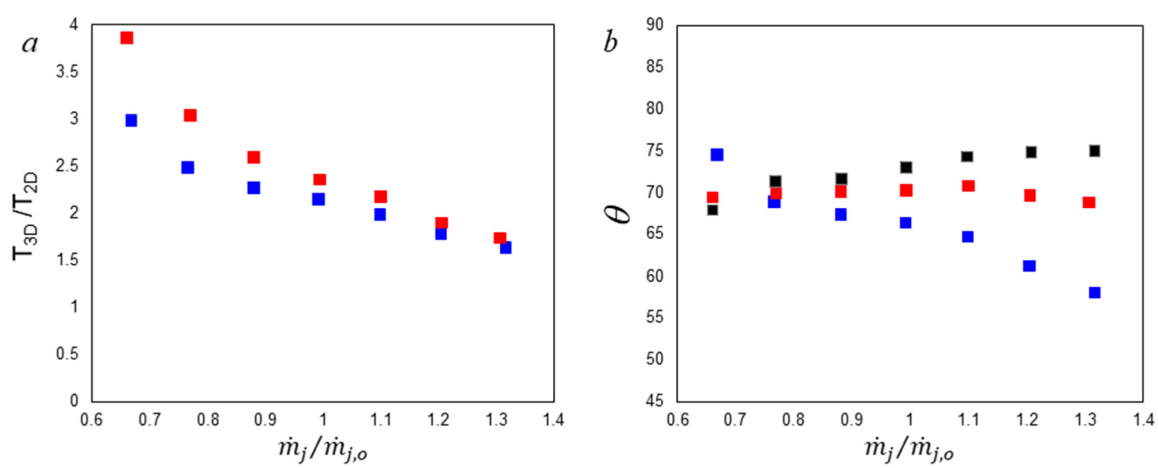

Figure 4. *Variations with normalized actuation mass flow rate $\dot{m}_j/\dot{m}_{j,o}$ of a) the ratio of the measured forces of the 2- and 3-D jet modules developed on the same Coanda surface T_{3D}/T_{2D}, and b) the angle of the resultant force θ relative to the streamwise (-x) direction: C2D-2 (■), C3D-1 (■), and C3D-2 (■).*

of the 2- and 3-D jet modules T_{3D}/T_{2D} are shown in Figure 4a. These data show that the lower active area of the 3-D wall jets (C3D-1 and -2 are $0.041A_{2D-2}$ and $0,035A_{2D-2}$, respectively) leads to induced forces at a given mass flow rate that within the present range of $\dot{m}_j$ are significantly higher than the corresponding Coanda force of the 2-D jet although this ratio decreases with increasing mass flow ratio (see also Figure 6). An assessment of the variation of the azimuthal attachment of the 2- and 3-D wall jets to the Coanda surface with $\dot{m}_j/\dot{m}_{j,o}$ is shown in Figure 4b in terms of the angle of the resultant force θ relative to the streamwise (x) direction (by this measure, $\theta = 90^{\circ}$ corresponds to full vertical turning of the actuation jet on the Coanda surface). These data show that the azimuthal attachment of C2D-2 increases monotonically from 68º to 75º as the mass flow rate nearly doubles while for configuration C3D-2 θ is nearly invariant with a local maximum of 70º at $\dot{m}_j/\dot{m}_{j,o} = 1.1$. However, for C3D-1 ($A_{\text{jet}} = 0.034A_1$) θ decreases monotonically with $\dot{m}_j/\dot{m}_{j,o}$ from 75º to 58º suggesting that the attachment of the 3-D jets improves with the larger orifice spanwise aspect ratio of C3D-2 (AR = 3) and may even be impeded by spanwise interaction between adjacent jets in C3D-1. Overall, the data for C3D-2 indicate that arrays of discrete wall jets can yield higher Coanda force compared to the 2-D wall jet and remain reasonably well attached to the Coanda surface.

The flow control modules that were integrated into the wind tunnel model were designed based on the bench-test results (cf. Figure 4). As noted above, the aerodynamic performance was tested in two primary spanwise configurations. In the first configuration the active spanwise extent of the actuation was restricted to the center 1/3 segment of the airfoil's span and the aerodynamic performances of the 2-D configurations C2D-1 (active area A_{2D-1}) and C2D-2 ($A_{2D-2} = 0.82A_{2D-1}$) were compared with configurations C3D-1 and C3D-2 whose active areas were $0.34A_{2D-1}$ and $0.29A_{2D-1}$ respectively. In the second spanwise configuration the active spanwise extent of the actuation occupied the entire span of the 2-D model and the aerodynamic performances of the 2-D and various 3-D configurations were compared and scaled relative to the 1/3 span segment. Some details of configurations C2D-2, C3D-1 and C3D-2 are shown for reference in Figures 5a-c (top views) and 5d-e (side views). The top views in Figures 5a-c show the respective top views of the 2-D jet and the spanwise arrays of 29 and 14 equally spaced fluidic oscillators. The corresponding side view show sections of the 2-D jet (Figure 5d) and through the center of the 3-D jet orifice (Figures 5e). As in the original design of Englar et al., the 2-D wall jet is driven directly from the upstream inner plenum and issues tangentially to the Coanda surface. As shown in Figure 5e, the 3-D orifices are higher than the 2-D

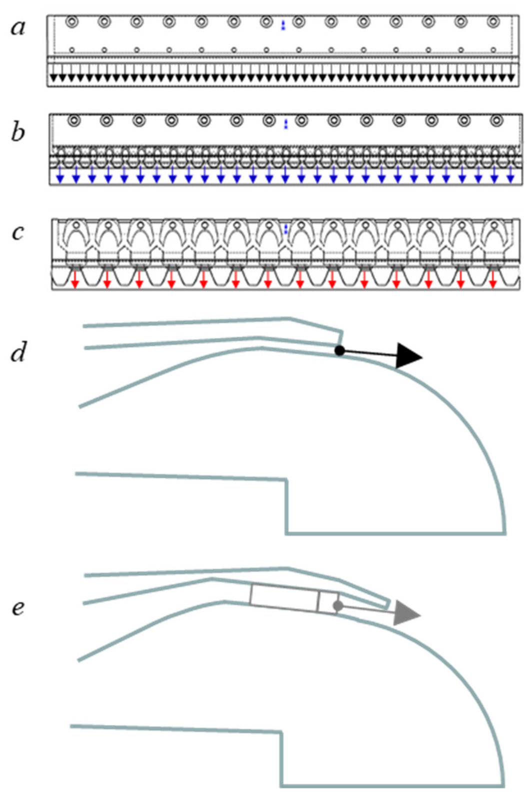

Figure 5. *Top views of the C2D-2 (0.82A_1, a), C3D-1 (0.34A_1, b), and C3D-2 (0.29A_o, c), and representative cross-sectional views of the 2-D (d) and 3-D (e) actuation modules integrated in the airfoil's trailing edge (cf. Figure 1b).*

orifice (up to three-fold) and they issue at the nearly the same azimuthal position along the Coanda surface. Measurements were conducted with 2- and 3-D actuation using both the central actuation module ($L_{act} = L/3$, cf. Figure 1b) with inactive modules having the same cross-sectional area on either side of the active module, and actuation along the full span of the airfoil.

IV. Circulation Control

The Coanda forces of the 2- and 3-D wall jet actuators *when installed at the central 1/3 span segment of the airfoil's trailing edge in the wind tunnel* in the absence of cross flow are shown in Figure 6 by considering the variation of C_μ with C_q using a tunnel reference speed of 35 m/sec. It can be shown that absent compressibility effects, $C_\mu \sim C_q^2$ and so Figures 6a-c show these variations for the total C_μ (based on T) and $C_{\mu-y}$ $C_{\mu-x}$ (corresponding to T_y and T_x). Figure 6a shows that for both the 2- and 3-D wall jets C_μ varies nearly linearly with C_q^2 over the entire range tested. For the 2-D jets there is a slight increase in the rate of change of C_μ for CD2-2 compared to CD2-1 as a result of its smaller exit area ($0.82A_{2D-1}$), within the test range. However, the Coanda forces developed by the arrays of the fluidic oscillators are higher than the corresponding forces developed by the 2-D jets especially for C3D-2 (e.g., for $C_q = 1{\cdot}10^{-2}$ C_μ for CD3-2 is nearly 85% higher than for CD2-1) although as noted in connection with Figure 4, the ratio between the Coanda forces diminishes with increasing actuation mass flow rate. More insight into effectiveness of the momentum generation by these actuators is gained when the Coanda force T in Figure 6a is decomposed to yield $C_{\mu-y}$ and $C_{\mu-x}$ (corresponding to T_y and T_x, in Figures 6b and c, respectively). First, the pairs of vertical and horizontal components of the forces effected by C2D-1 and -2 are each nearly equal indicating approximately the same turning about the Coanda surface, and because T_y/T_x is somewhat higher for the 2-D jets also indicates that they attach to the surface somewhat farther than the 3-D jets. It is remarkable that even though the internal designs of the two 3-D jet configurations are different, they generate nearly identical horizontal force components that are higher relative to the horizontal force of the 2-D jets. While the vertical force

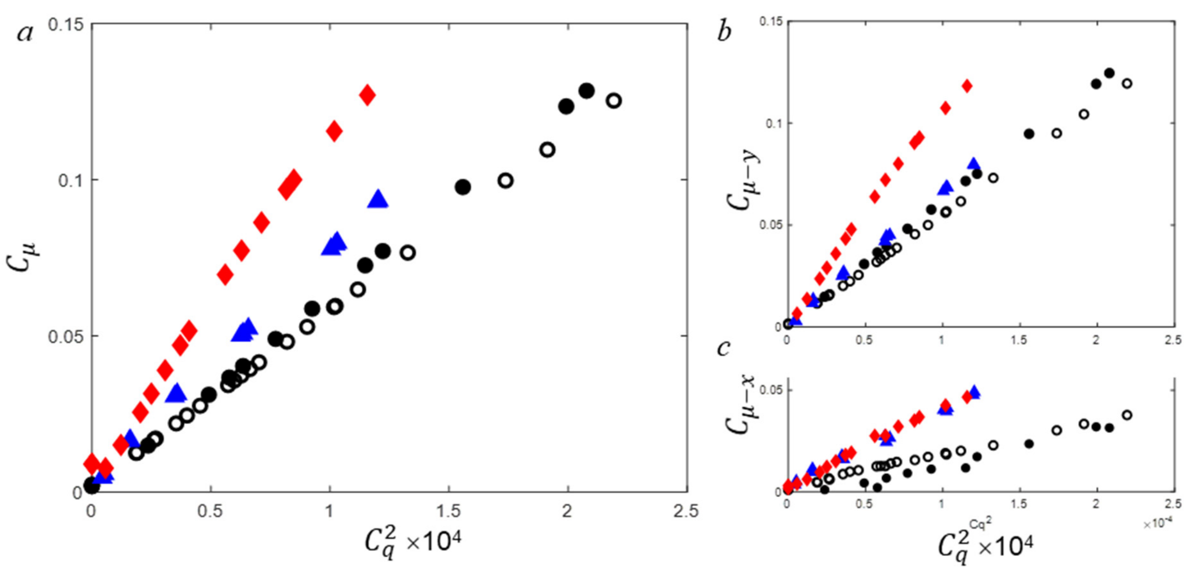

Figure 6. *Variation with the actuation mass flow rate C_q of (a) C_μ based on the magnitude of the measured Coanda force T, and (b) and (c) corresponding momentum coefficients $C_{\mu-y}$ (b) and $C_{\mu-x}$ (c) of the vertical and horizontal components of the Coanda force T_y and T_x, , respectively:* ***C2D-1 (A_1, ○), C2D-2 (0.82 A_1, ●), C3D-1 (0.34 A_1, ▲),*** *and* ***C3D-2 (0.29 A_1, ♦)****.*

produced by C3D-1 is only slightly higher than the corresponding component for the 2-D jets, C3D-2 produces higher vertical thrust indicating higher turning angle (cf. Figure 4).

The aerodynamic performance of the Coanda effects of the 3-D jets at the trailing edge of the current airfoil model is compared with the 2-D jets in Figures 7 in terms of the variation with C_μ and C_q of the induced lift increments ΔC_L relative to the baseline levels (in the absence of actuation) in Figures 7a and b, respectively for $Re = 4.7 \cdot 10^5$ (ΔC_L is normalized by the active spanwise area of the wing). The data in Figure 7a are shown at $\alpha = -5^o$, 0^o, and 5^o and for each actuator configuration exhibit a nearly-linear variation of ΔC_L with C_μ in two distinct rates below and above $C_\mu \approx 0.06$. This change in the rate of variation of ΔC_L with C_μ was observed by a number of earlier investigators (e.g., Jones, 2005, Radespiel et al., 2016) who argued that it results from transition from "boundary layer (or separation) control" to "circulation control" (of course, in either regime the change in induced lift is associated with a change in circulation). The present data show that while in the "separation control" regime ($C_\mu < 0.06$) all wall jets yield nearly-identical performance and the same rate of change of ΔC_L with C_μ, the departure between their performances in the "circulation control regime is approximately offset by some constant while the nearly linear rates of increase of ΔC_L with C_μ are almost identical. This finding indicates that each of these wall jets reaches a different upper limit of its separation control on the Coanda surface and the increase in circulation or lift thereafter is manifested primarily by turning of the outer flow over the Coanda surface. These data also show that although the magnitudes of ΔC_L effected by the 2- and 3-D actuators are not the same, the effect of each actuator exhibits little or no variation with small angles of attack.

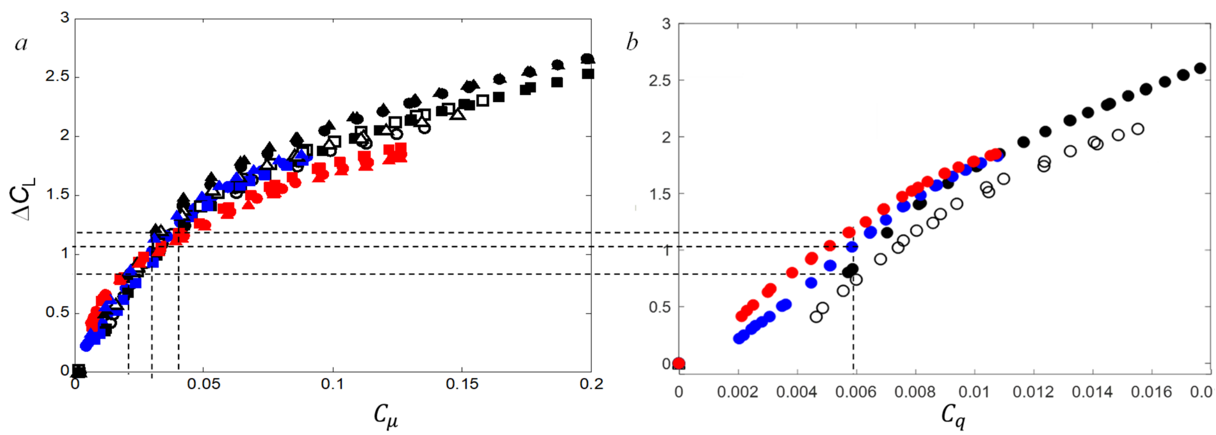

Figure 7. *The variation with C_μ (a) and C_q (b) of the lift increments ΔC_L effected by the Coanda trailing edge circulation control of the airfoil model using 2- and 3-D jets ($Re = 4.7 \times 10^5$) at $\alpha = -5^o$ (**triangle**), 0^o (**circle**), and 5^o (**square**): **C2D-2 (0.82 A_1**, black), **C3D-1 (0.34 A_1**, blue), and **C3D-2 (0.29 A_1**, red).*

The variation of ΔC_L with C_q in 7b shows an interesting trend in terms of the changes in ΔC_L (for clarity, the data in Figure 7b are restricted to $\alpha = 0^o$ only). Although not as distinct as the variation of ΔC_L with C_μ, these data show some indications of the "boundary layer control" and "circulation control" regimes for each actuator, but unlike the data in Figure 7a, the corresponding data in Figure 7b do not overlap, the transition between the two regimes occurs at different levels of C_q, and the rates of change of ΔC_L with C_q are not the same within the boundary layer control regime. The rates of ΔC_L induced by C2D-2 and C3D-1 and –2 around $C_q \approx 0.009$ are nearly identical and appear to increase linearly with C_q. Within the range $C_q < 0.009$ the data in Figure 7b show that for a given C_q the 3-D jets induce higher ΔC_L and C_μ than the 2-D jets. For example, at $C_q = 0.006$

ΔC_Ls for C2D-2 and C3D-2 are 0.84 and 1.18, respectively, while the corresponding 2- and 3-D C_μs are 0.018 and 0.036. It should be noted that even when ΔC_L is the same for C2D-2 and C3D-1 and -2 for $C_q > 0.009$, *C_μ of the 3-D jets is significantly higher than for the 2-D jets*. For example, at $C_q = 0.01$, ΔC_Ls for C2D-2 and C3D-2 are about 1.75 but the corresponding 2- and 3-D C_μs are about 0.06 and 0.15 (*nearly double*).

The variation with actuation momentum coefficient of the drag increments ΔC_D effected by the 2- and 3-D trailing edge circulation control relative to the corresponding baseline levels in the absence of actuation are compared in Figure 8. The variation of the drag increments associated with the 2-D jets with C_μ for each α follows the trend exhibited by ΔC_L in Figure 7a, namely a nearly-linear increase in two distinct rates below and above $C_\mu \approx 0.06$ (corresponding to BL control and circulation control), but unlike the trend of ΔC_L, the respective rates of ΔC_D of the 2-D jets increase significantly with α. For example, at $C_\mu = 0.1$ $\Delta C_D = 0.094$ at $\alpha = 0^o$, increases by about 45% (to 0.135) and decreases by about 33% (to 0.062) at $\alpha = +5^o$ and -5°, respectively. It should be noted, however, that while ΔC_D of the 2-D jets continues to increase with C_μ at $\alpha = 0^o$ and 5°, at $\alpha = -5^o$ ΔC_D asymptotes to about 0.067 while as is evident from Figure 7a, the corresponding lift increment continues to increase).

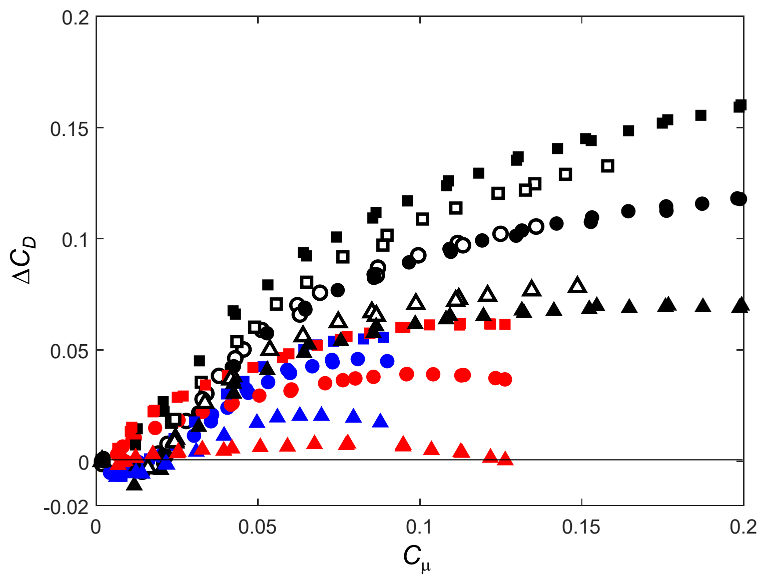

***Figure 8.** As in Figure 7, the variation with C_μ of the drag increments ΔC_D associated with the Coanda effects trailing edge circulation control of the airfoil mode using 2- and 3-D jets ($Re = 4.7\cdot10^5$) at $\alpha = -5^o$ (**triangle**), 0^o (**circle**), and 5^o (**square**): **C2D-2 (0.82 A_1**, black), **C3D-1 (0.34 A_1**, blue), and **C3D-2 (0.29 A_1**, red).*

Perhaps the most salient feature of the data in Figure 8 is that within the range of operation of the 3-D jets in the present investigations ($C_\mu < 0.126$ for C3D-2), the drag increments induced by their actuation for a given C_μ are significantly lower than the corresponding increments induced by the 2-D jets. For example, for C3D-2 at $C_\mu = 0.1$ $\Delta C_D = 0.01$, 0.039, and 0.062 at $\alpha = -5^o$, 0° and +5°, respectively and the corresponding drag increments induced by the 2-D jets are about 54%, 58%, and 62% *higher*. As a result, the ratios of the actuation induced lift and drag increments for the 2-D (C2D-2) and 3-D (C3D-2) actuations at $\alpha = 0^o$ and $C_\mu = 0.1$ are about 21 and 43, respectively indicating that *the 3-D actuation at the same momentum coefficient is significantly more efficient.* Furthermore, as shown in Figure 8, for $C_\mu > 0.06$ the induced drag by the 3-D actuation at $\alpha = 0^o$ and 5° asymptotes to the levels mentioned above while ΔC_L continues to increase while the drag at $\alpha = -5^o$ begins to decrease with increasing C_μ and ultimately vanishes. Also of note is the slight reduction of the baseline drag ($\Delta C_D < 0$) in the range $C_\mu < 0.02$ for both the 2- and 3-D configurations that are ostensibly associated with enhanced attachment on the Coanda surface at low levels of the momentum coefficient.

The mechanisms that lead to these striking differences in aerodynamic performance between 3-D actuation and the corresponding 2-D actuation have not been fully explored as part of the present investigations and are currently being studied separately. The preliminary results indicate that the reductions in actuation induced drag is attributed to the interaction of the cross flow with the discrete fluidically oscillating wall jets over the Conada surface that gives rise to the formation of surface-bound array of counter-rotating streamwise vorticity concentrations in contrast to strong edge vortices that are induced by the 2-D jets at the spanwise edges of the active actuation segment. Some of the mechanisms associated with similar 3-D actuation were explored earlier in the works of DeSalvo et al. (2016, 2020) who investigated high lift enhancement by the Coanda effect of a spanwise array of fluidically-oscillating wall jets over the curved surfaces of simple flaps. Furthermore, it is noted in connection with Figure 6 that the Coanda force induced by C3D-2 is larger than the corresponding force effected by the 2-D jets and that in fact both the cross stream and streamwise components of the force induced by the 3-D wall jets are significantly larger than the corresponding components induced by the 2-D jets.

As noted above, the measurements described in Figures 7 and 8 were performed with actuation modules over the center 1/3 segment of the wing model (i.e., $L_{act} = L/3$ with identical inactive trailing edge at each outboard segment). Following the measurements shown in Figures 7 and 8, the configurations C3D-1 and -2 were expanded to the full span ($L_{act} = L$) and their aerodynamic effects were compared with the 2-D wall jet C2D-1. Figures 9a and b compare the performance of the actuation for $L_{act} = L/3$ and L in terms of the variation with C_μ of the induced lift and drag increments, respectively, where each distribution is scaled by its active fraction of the span. In these plots, the induced drag is represented using the earlier approach of Jones and Englar (2003) and Jones (2005) in which the circulation-induced drag increment $\Delta C_{D,cir}$ is computed by *subtracting* the streamwise component of the thrust Coanda force coefficient $C_{\mu\text{-}x}$ effected by the 2- and 3-D wall jets that is measured in the absence of cross flow (cf. Figure 6).

The lift increments effected by 2- and 3-D actuation in Figure 9a exhibit similar trends to the corresponding data in Figure 7, are nearly invariant with α (at least within the present range) and show a good agreement between the scaled full- and 1/3-span actuation despite the obvious 3-D

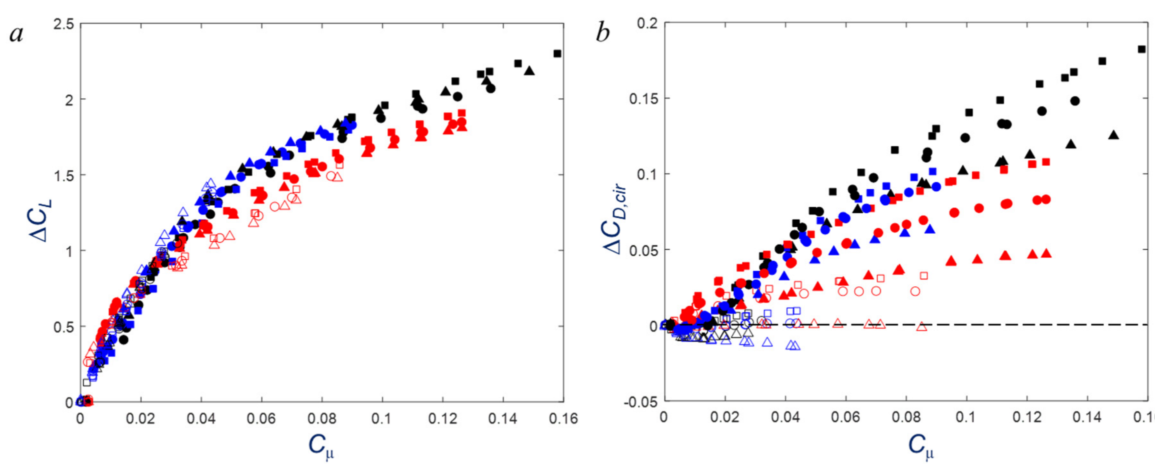

Figure 9. *The variation with C_μ of the lift and effective drag increments ΔC_L (a) and $\Delta C_{D,cir}$ (b), respectively associated with circulation control along the full span (L, open symbols) and span segment (L/3, solid symbols) using 2-D and 3-D actuation ($Re = 4.7 \cdot 10^5$) at $\alpha = -5^o$* ***(triangle)****, 0^o* ***(circle)****, and 5^o* ***(square)****:* ***C2D-2 (0.82 A_1,*** *black),* ***C3D-1 (0.34 A_1,*** *blue), and* ***C3D-2 (0.29 A_1,*** *red).*

effects that are associated with the latter. That ΔC_L effected by C3D-2 is somewhat lower for the full span actuation may be attributed to the small number of active actuators in the $L/3$ span segment. As discussed in connection with Figure 8, unlike the near-invariance of the lift increments with α, the circulation-induced drag increment $\Delta C_{D,cir}$ increase with α for both the full- and fractional-span actuation showing the sensitivity of the induced drag to the changes in boundary layer thickness with α on the suction side of the airfoil. More importantly, Figure 9b shows that $\Delta C_{D,cir}$ is significantly *higher* for fractional- than for full-span actuation underscoring the importance of spanwise edge effects associated with the former. However, as emphasized in the discussion of Figure 8, fractional-span actuation the interaction of the cross flow with a sparse spanwise array of 3-D wall jets results in significantly *lower* drag increments compared to the corresponding 2-D wall jets. As already noted, compared to fractional-span actuation, full-span 2- and 3-D actuation results in lower $\Delta C_{D,cir}$ that varies only weakly with α. While full-span actuation by the C2D-1 and C3D-1 wall jets leads to nearly negligible changes in $\Delta C_{D,cir}$ (in fact, C3D-1 results in a small decrement at $\alpha = -5^o$), full-span C3D-2 actuation results in small increases in $\Delta C_{D,cir}$ at $\alpha = 0$ and $+5^o$ that become asymptotic around $\Delta C_{D,cir} \approx 0.025$ with increasing C_μ. These differences in $\Delta C_{D,cir}$ between C3D-1 and -2 indicate that the spacing and strength of the spanwise array of streamwise vortices induced by the 3-D wall jets can probably be optimized to minimize the induced drag.

IV. Scaling of Actuation Layout

The present investigations also considered the sensitivity of the aerodynamic performance of the 3-D fluidically-oscillating wall jet arrays to some variations in scaling the actuators spacing and of the jet orifices in the array's exit plane. These studies utilized the basic design of the fluidic oscillator array C3D-1 and the effects of variations of its geometry characteristics were compared with the 2-D Coanda jet (as shown in Figure 6, for a given C_μ the performances of C2D-1 and -2 are nearly identical). First, the effects of the aspect ratio of the jet orifices (AR = 1, 2 and 2.5) were considered while keeping the orifice height above the Coanda surface h (and the ratio h/R) as well as the array's total spanwise active area invariant. With this scaling of the orifice aspect ratio the active trailing edge segment included 29, 14, and 11 wall jet modules with nearly identical respective total active areas ($0.34A_1$, $0.33A_1$, and $0.32A_1$). Similar to the procedure used in connection with Figure 6, the variation of the Coanda forces with actuation mass flow rate was measured in the absence of cross flow in the tunnel and the total forces are shown in Figure 10a for the 2- and 3-D jets. While the orifice areas of the 3-D jet arrays are clearly smaller than the area of the 2-D array, it is interesting to note that the rates of change of C_μ with C_q^2 increase with the jets' aspect ratio even though the total active areas of the arrays are the same indicating that increasing the spanwise width or aspect ratio of the 3-D actuation jet enhances its interaction with the Coanda surface (although this effect clearly diminishes in the limit of a 2-D jet indicating saturation associated with spanwise interference). This interaction with the Coanda surface is also manifested by the angles θ of the resultant forces relative to the streamwise (x) direction. For example, for $C_q = 0.01$ even though the vertical component of the Coanda force is higher for the 3D jet with $AR = 2.5$, turning of the 2-D jet is higher: $\theta = 74^o$ and 59^o for the 2-D and C3D-1($AR = 2.5$), respectively.

The aerodynamic effects associated with the different aspect ratios of 3-D wall jets are shown in Figure 11 at $\alpha = 0^o$. Interestingly, as shown in Figure 11a, for a given C_μ the induced lift increment appears to diminish with increasing jet aspect ratio when the total active area of the 3-D actuation

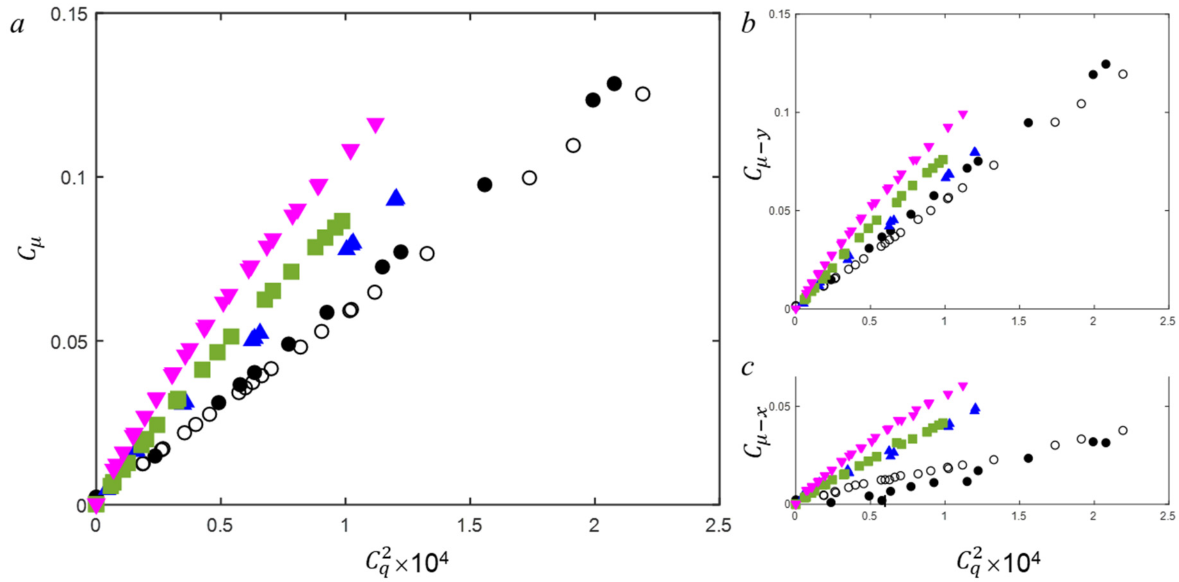

Figure 10. *As in Figure 6 for **C2D-1** (**A_1**, ○) and **C2D-2** (**$0.82A_1$**, ●) that are compared with three aspect ratio variants of **C3D-1** (**AR= 1**, **$0.34A_1$**, ▲), **C3D-1** (**AR=2**, **$0.34A_1$**, ■), and **C3D-1** (**AR=2.5**, **$0.32A_1$**, ▼).*

is preserved even though its effected Coanda force increases with *AR* (Figure 10a). In fact, it is noteworthy that as shown in Figure 9, an array of 14 similar 3-D jets (C3D-2) with $AR = 3$ (and somewhat smaller total active area) yielded *lower* ΔC_L than the present 14 jet array with $AR = 2$ (1.7 vs. 1.5 at $C_\mu = 0.1$). It is conjectured that since C_μ/jet is nearly the same for the two 14-jet arrays that the somewhat lower ΔC_L is associated with the lower momentum density of the higher aspect ratio jets. However, as shown in Figure 11b, since the corresponding induced drag increments also decrease with increasing aspect ratio, $\Delta C_L/\Delta C_{D,cir}$ increases with increasing *AR* (for example, at $C_\mu = 0.1$ $\Delta C_L/\Delta C_{D,cir} \approx 1.5$ and 2 for the 2-D and 3-D $AR = 2.5$-actuation). The effectiveness of the actuation is depicted in Figure 11c by considering the incremental change in lift $\Delta C_{L,jet}$ and the corresponding momentum coefficient per actuation jet. For $C_{\mu,jet} < 0.03$, actuation with $AR = 1$ and 2 appears to induce about the same $\Delta C_{L,jet}$ while $AR = 2.5$ is somewhat less effective (its rate of increase with C_μ/jet is lower). The lift induced by $AR = 1$ (smallest scale

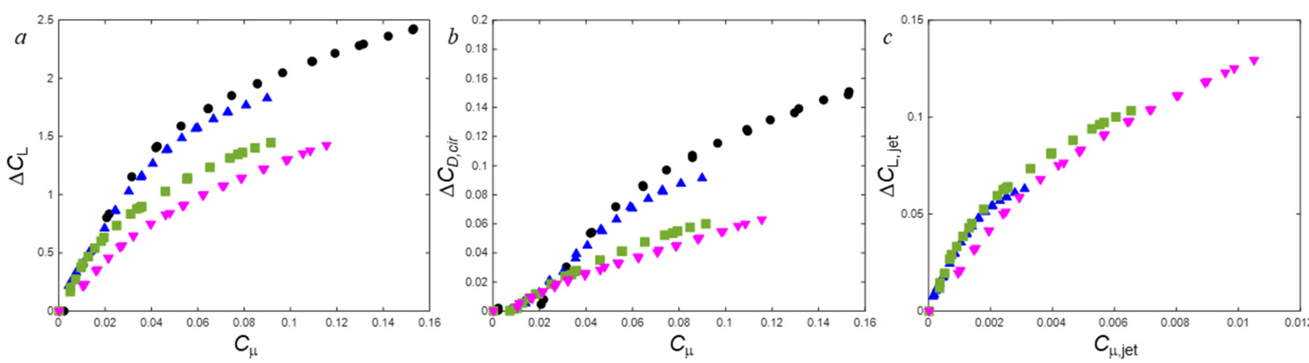

Figure 11. *Variation with C_μ of ΔC_L (a) and $\Delta C_{D,cir}$ (b) and of the lift increment per active jet with C_μ per active jet (c) for 3-D jets at $\alpha=0^o$ ($Re = 4.7 \cdot 10^5$) with different orifice aspect ratios: **C3D-1** (**AR= 1**, **$0.34A_1$**, ▲), **C3D-1** (**AR=2**, **$0.34A_1$**, ■), and **C3D-1** (**AR=2.5**, **$0.32A_1$**, ▼), compared with **C2D-2** (**$0.82A_1$**, ●).*

orifice) appears to depart from the 'BL control' domain at C_μ/jet ≈ 0.003 indicating an upper performance limit that is probably associated with interference between adjacent jets in this dense array (29 jets). Next, $AR = 2$ (14 jets) appears to remain somewhat longer in the 'BL control' domain, thus elevating the circulation-control effect beyond that of $AR = 1$ jets, while for $AR = 2.5$ (11 jets) ΔC_L/jet is not locally as efficient in the BL control, but continues to increase nearly linearly with C_μ/jet in the circulation control domain without indication of subsiding within the measurement range. These data indicate that under scale constraints that may hinder the performance an array of the fluidic actuators the aerodynamic performance of the actuation in terms of ΔC_L/jet at increased momentum coefficient may be optimized by considering increased actuator aspect ratio that yields higher performance at higher C_μ/jet.

Another scale characteristic of 3-D jet arrays is the effect of the spanwise density or the spacing of the jet modules on their aerodynamic performance. As noted by DeSalvo et al. (2016), the performance can be affected by the available C_μ/jet and may result in higher lift increment (although the performance of closely spaced jets may also be hindered by spanwise interference). The effect of the jet spacing when the actuation modules are unchanged is investigated using spanwise arrays of configuration C3D-1 that are equally distributed at three characteristic spanwise spacings of their centerlines $s/c = 0.041$, 0.063, and 0.085 yielding 29, 19, and 14 jet modules within the actuated central 1/3 span segment for which the total active areas are $0.34A_1$, $0.22A_1$, and $016A_1$. Similar to Figures 6 and 10, the Coanda forces generated by the jet arrays in the absence of cross flow are shown in Figure 12a and compared with the corresponding 2-D jet C2D-1. These data show that for a given C_μ, the Coanda forces induced by the 3-D arrays are larger than the force induced by the 2-D wall jet (C2D-1) and similar to C3D-1 and -2 in Figure 6, increase with the spacing of the 3-D wall jets. Furthermore, for a given C_q, the Coanda force increases nearly linearly with C_q/jet indicating that within this parameter range at a given C_q/jet the total force (as measured by C_μ) is nearly a multiple of the force induced by each of the jets within the array. Figures 12b and c show that the angles θ of the resultant Coanda forces relative to the streamwise (x) direction increases with s/c - indicating that a sparse jet arrays can, in

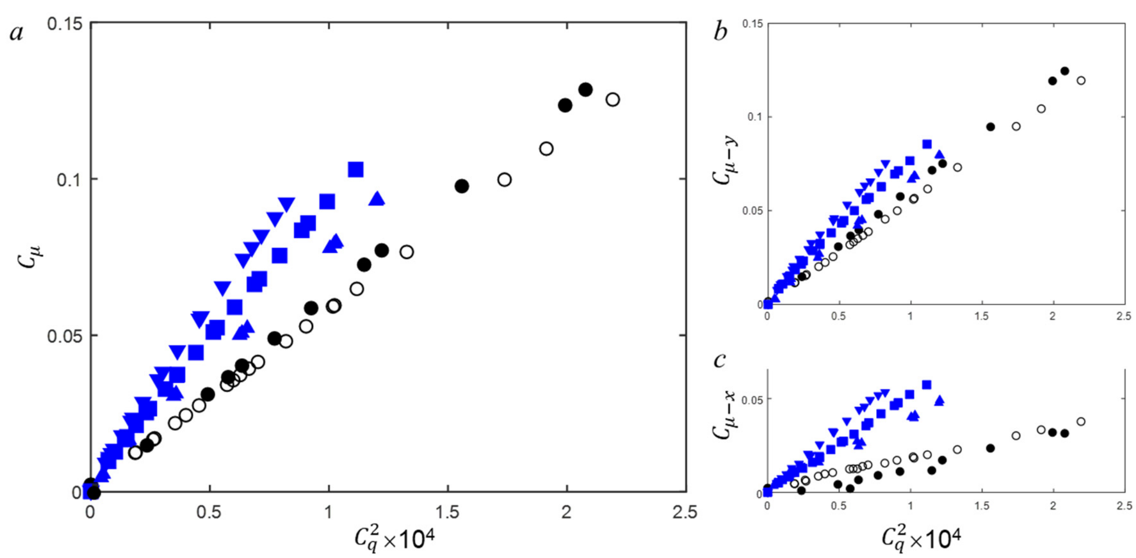

Figure 12. *As in Figure 6 for* ***C2D-2 (0.82A*****$_1$**, ●*) that is compared with three* ***C3D-1*** *arrays having different jet spacings s/c = 0.041, (▲), 0.063 (■), and 0.085 (▼).*

principle, achieve the same turning over the Coanda surface as a dense jet array at some higher C_μ/jet.

The effects of varying the spanwise spacing of the actuation jets on the induced aerodynamic loads at $\alpha = 0^o$ are depicted by considering the variation of ΔC_L with the array's C_μ in Figure 13 (the data for the 2-D jet C2D-1 are also included for reference). Comparison of these data with Figure 9 (in which the data for C2D-1 and for C3D-1 $s/c = 0.041$ also appear) shows that while for $C_\mu < 0.03$ ΔC_L for all the arrays are identical, for $C_\mu > 0.03$ (the circulation control regime) ΔC_L increases nearly linearly with C_μ, but at different rates that for a given C_μ diminish with increasing s/c despite the increase in C_μ/jet. Considering that the jets in these arrays are identical, the data in Figure 13a indicate that the reduction in the rate of increase of ΔC_L with C_μ simply indicates the limitation in the effectiveness of individual jets within the array to increase the circulation by turning of the cross flow between the neighboring jets, and that to increase the circulation further would require additional jets. Considering the spanwise actuation density of the three 3-D arrays, the aerodynamic performance data in Figure 13a is scaled with respect to the number of active jets in each array and the variation of $\Delta C_{L,jet}$ with $C_{\mu,jet}$ is plotted Figure 13b. These data show that scaling the aerodynamic performance of arrays of identical jets and their total momentum coefficient in terms of their active jets yields a single curve that appears to depict a universal dependence that allows for direct relationship between arrays of different actuation density.

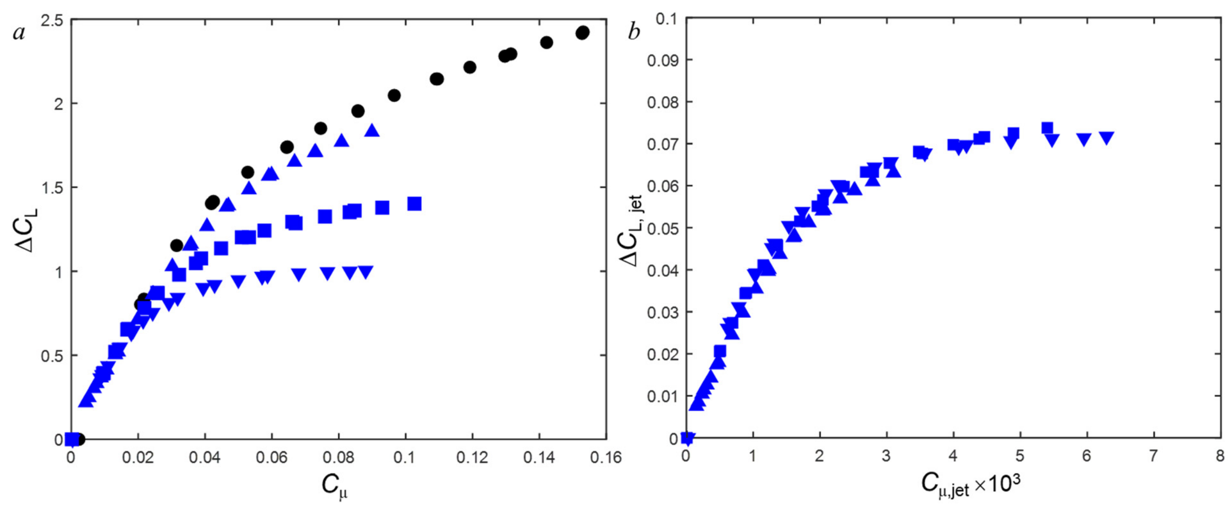

Figure 13. *The variation with C_μ of the lift increments ΔC_L at $\alpha=0^o$ (a) for three spanwise equally distributed arrays of configuration C3D-1 where each uses the same jet module at three characteristic spanwise spacings s/c = 0.041, (▲), 0.063 (■), and 0.085 (▼) yielding 29, 19, and 14 jet actuators within the central 1/3 span segment of the airfoil such that the total active areas are $0.34A_I$, $0.22A_I$, and $016A_I$. The per active jet lift coefficient increment $\Delta C_{L,jet}$ and momentum coefficient $C_{\mu,jet}$ are shown in (b).*

The dependence of the aerodynamic performance on the spanwise density and the aspect ratio of actuation jet arrays shown in Figures 11c and 13b indicates scaling dependence on two ratios namely the area ratio of the arrays active area to some reference area A/A_{ref} and the actuation duty cycle as measured by the ratio of the jet span to the spanwise periodicity of the array w/s. It is noted that A_{ref} can be taken to be the area of the reference 2-D jet in the present investigations or could also be the active spanwise planform area of the wing. Based on the findings associated with Figures 11 and 13, it is argued that *for a given Coanda surface* the aerodynamic performance as measured by ΔC_L and C_μ should depend on the jet orifice parameter, expressed by its cross-

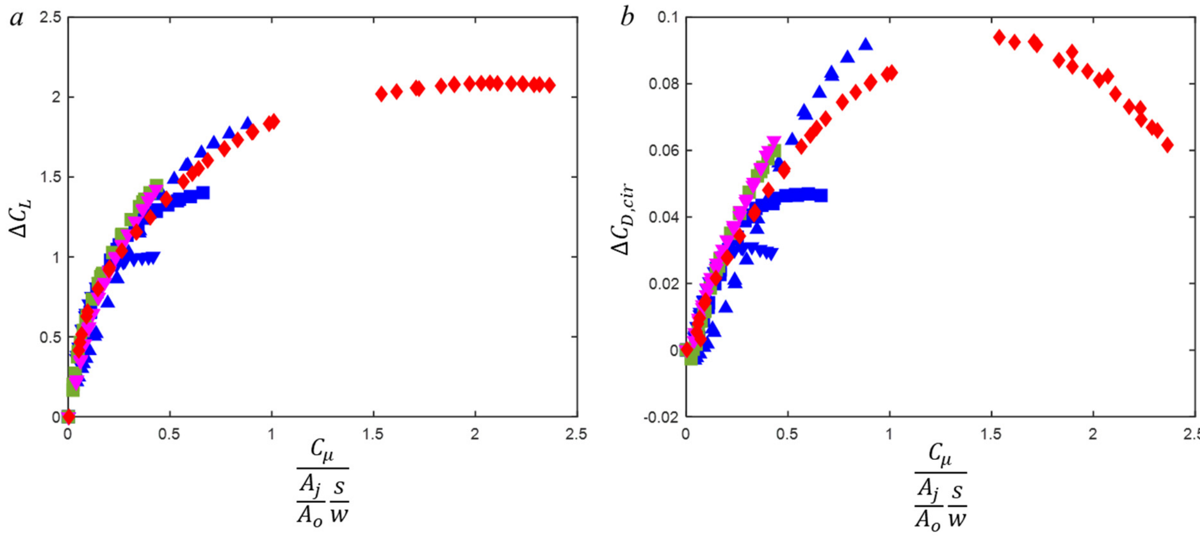

Figure 14. *Increment in total lift (a) and circulation drag (b) coefficient relative to the total jet momentum coefficient and relative jet orifice area A_j and spacing s for the varying* ***C3D-1*** *spacing s/c = 0.041 (▲), 0.063 (■), and 0.085 (▼), for its increased aspect ratio* ***C3D-1*** *(AR=2, ■), and* ***C3D-1*** *(AR=2.5,▼), and for* ***C3D-2*** *(♦).*

sectional area A_j, the orifice linear dimension, expressed by its width *w*, and the linear jet spacing *s* in the jet array. Following this argument, the dependence of ΔC_L on C_μ is scaled such that $\Delta C_L = f[C_\mu \cdot (A_j/A_o)^{-1} \cdot (s/w)^{-1}]$. This scaling is tested by considering all the 3-D jet arrays utilized in the present experiments with varying spacings and orifice areas. The variation of the lift coefficient with the scaled momentum coefficient is shown in Figure 14a for $\alpha = 0^{o}$. These plotted data exhibit remarkable collapse, and clearly depicts the two control regimes namely BL control and circulation control as discussed in connection with Figure 7. It is clearly noted that for the two arrays C3D-1 (s/c = 0.063, and 0.085), ΔC_L begins to deviate from the curve envelope at $C_\mu \cdot (A_j/A_o)^{-1} \cdot (s/w)^{-1} = 0.25$ and 0.45. This is indicative of local saturation of the Coanda effect of the individual jets and that the jets are simply too far apart hindering the flow turning of circulation control between neighboring jets. Although the dependence of the drag coefficient on the scaled C_μ is somewhat more scattered, Figure 14b shows that even ΔC_D has about the same dependence on the scaled C_μ as ΔC_L. It is interesting to note that Figure 14b predicts that the induced drag over the present Coanda surface has a local maximum and thereafter diminishes even though the lift increment continues to increase weakly.

V. Conclusions

Lift increments on an airfoil by controlled modification of its circulation using the Coanda effect on a bluff trailing edge are investigated in low-speed wind tunnel experiments ($4.7 \cdot 10^5 < Re < 6.1 \cdot 10^5$) at low angles of attack ($-5° < \alpha < 5°$). While in earlier investigations Coanda-based circulation control was commonly applied using a nominally 2-D steady tangential wall jet, the present study builds on earlier high-lift implementation of fluidic actuation over a simple flap by spanwise arrays of 3-D fluidically oscillating wall jets with varying spanwise distributions and scaling (DeSalvo et al., 2016, 2020). The primary objective of the present work is to enhance three-dimensional spanwise-segmented circulation control by a conventional 2-D wall jet on a quarter-cylinder Coanda surface using spanwise arrays of 3-D fluidically oscillating jets at the same operating conditions. The present investigation also compares the effects of the 2- and 3-D Coanda actuation over a spanwise segment of the airfoil with actuation over its entire span.

Following bench testing of several configurations of spanwise arrays of fluidically oscillating jets, jet arrays were installed in a modified 2-D NASA 17%-thick supercritical airfoil and the streamwise and cross stream components of the induced Coanda forces by 2- and 3-D wall jets were measured in the absence of cross flow over a range of actuation mass flow rates. It was shown that the Coanda forces vary linearly with the square of the actuation mass flow rate or that $C_\mu \sim C_q^2$, and yielded at least twice the thrust of the 2-D continuous jet while maintaining comparable attachment to the Coanda surface.

The aerodynamic performance of the Coanda effects of the 3-D jets at the central (one-third) span segment of the trailing edge of the airfoil model was compared with the 2-D jets in terms of the variation with C_μ and C_q of the induced lift increments ΔC_L relative to the baseline levels in the absence of actuation. Similar to the findings of earlier investigators, these data exhibited nearly-linear variation of ΔC_L with C_μ in two distinct regimes namely, boundary layer (or separation) control and circulation control. While in the separation control regime ($C_\mu < 0.06$) the 2- and 3-D wall jets yielded nearly identical performance and the same rate of change of ΔC_L with C_μ, in the circulation control regime ΔC_L of the 2-D jets was somewhat higher but offset by a constant with nearly the same rates of increase with C_μ. These data also show that for a given C_q within the separation control regime the 3-D jets can induce higher ΔC_L and C_μ than the 2-D jets and that even when the induced ΔC_L is the same, C_μ of the 3-D jets is attained at lower C_q.

Perhaps more importantly, *the present investigations showed that within the range of operation of the 3-D jets, the induced drag increments by the actuation at a given C_μ are significantly lower than the corresponding increments induced by the 2-D jets*. For example, at $C_\mu = 0.1$ the drag increments induced by the 2-D jets are about 54%, 58%, and 62% higher than the 3-D jets $\alpha = +5^\circ$, 0°, and -5°, respectively indicating that the 3-D actuation at the same momentum coefficient is significantly more efficient. Preliminary results also indicate that the reductions in the actuation induced drag can be attributed to the interaction of the cross flow with the discrete fluidically oscillating wall jets over the Conada surface that gives rise to the formation of surface-bound array of counter-rotating streamwise vorticity concentrations in contrast to strong edge vortices that are induced by the 2-D jets at the spanwise edges of the active actuation segment.

The present investigations also considered the sensitivity of the aerodynamic performance of the 3-D wall jet arrays to some variations in scaling of actuator spacing and of the jet orifices in the array's exit plane. Based on measurements of the aerodynamic performance for several configurations of 3-D jet arrays, it is argued that the momentum coefficient that yields the aerodynamic performance for a given Coanda surface should be scaled by the actuation area ratio as measured by the ratio of the array's active area to some reference area A/A_{ref} and by its duty cycle as measured by the ratio of the jet orifice span to the spanwise periodicity of the array w/s. This scaling is tested by considering all 3-D jet arrays with varying spacings and orifice areas that were used in the present investigations. The variation of the lift coefficient with the scaled momentum coefficient exhibits remarkable collapse throughout the two control regimes (BL and circulation control). Nonetheless, deviation of ΔC_L from this collapse occurs with increasing jet spacing indicating an apparent saturation of the Coanda effect by jets that are too far apart. It is also shown that the drag increment ΔC_D has similar dependence on the scaled C_μ and the collapsed data suggests that the induced drag over the present Coanda surface has a local maximum and thereafter diminishes even though the lift increment continues to increase.

Acknowledgment
This research was developed with funding from the Defense Advanced Research Projects Agency (DARPA) Control of Revolutionary Aircraft with Novel Effectors (CRANE) Program. The views, opinions and/or findings expressed are those of the authors and should not be interpreted as representing the official views or policies of the Department of Defense or the U.S. Government.

References

Davidson, I.M., "The jet flap," *The Aeronautical Journal*, Vol. **60** (541), pp.25-50, 1956.

DeSalvo, M., Gissen, A., Whalen, E., and Glezer, A., "High-Lift Performance Enhancement of a Fowler Flap using Aerodynamic Flow Control," *AIAA Paper 2016-3306*, 2016.

DeSalvo, M., Whalen, E. and Glezer, A., "High-Lift Performance Enhancement Using Active Flow Control," *AIAA Journal*, Vol. **58** (10), pp. 4228-4242, 2020.

Dunham, J., "A theory of circulation control by slot-blowing, applied to a circular cylinder," *Journal of Fluid Mechanics*, Vol. **33** (3), pp.495-514, 1968.

Englar, R. J., "Application of Pneumatic Lift and Control Surface Technology to Advanced Transport Aircraft," in *Transportation Beyond 2000*, NASA, pp. 371-397, 1996.

Englar, R. J., "Circulation Control Pneumatic Aerodynamics: Blown Force and Moment Augmentation and Modification; Past, Present and Future," *AIAA Paper* 2000-2541, 2000.

Englar, R. J., "Overview of Circulation Control Pneumatic Aerodynamics: Blown Force and Moment Augmentation and Modification as Applied Primarily to Fixed-Wing Aircraft," NASA CP 2005-213509, 2005.

Englar, R. J., Hemmerly, R. A., Moore, W. H., Seredinsky, V., Valckenaere, W., and Jackson, J. A., "Design of the Circulation Control Wing STOL Demonstrator Aircraft," *Journal of Aircraft*, Vol. **18** (1), pp. 51–58, 1981.

Englar, R. J., Smith, M.J., Kelly, S.M. and Rover, R.C., "Application of Circulation Control to Advanced Subsonic Transport Aircraft, Part I: Airfoil Development," *Journal of Aircraft*, Vol **31** (5), pp 1160-1168, 1994.

Englar, Robert J. and Graham M. Blaylock, "Circulation Control Pneumatic Aerodynamics for High Lift, Flight Control and Cruise efficiency," Paper No. 1 at NATO AVT Control Effectors Workshop, High Lift 2 Session, May 2013.

Ghee, T.A. and Leishman, J.G., "Unsteady circulation control aerodynamics of a circular cylinder with periodic jet blowing," *AIAA Journal*, Vol. **30** (2), pp.289-299, 1992.

Jones, G. and Englar, R., "Advances in Pneumatic-Controlled High-Lift Systems through Pulsed Blowing," *AIAA Paper* 2003-3411, 2003.

Jones, G. S., "Pneumatic flap performance for a 2d circulation control airfoil, steady and pulsed," *Proceedings of the 2004 NASA/ONR Circulation Control Workshop, Part 2*, 2005.

Lockwood, V., "Lift Generation on a Circular Cylinder by Tangential Blowing from Surface Slots," *NASA TN D-244*, 1960.

Loth, J. and Boasson, M., "Circulation Controlled STOL Wing Optimization," *Journal of Aircraft*, Vol. **21** (2), pp. 128-134, 1984.

Neuendorf, R. and Wygnanski, I., "On a Turbulent Wall Jet Flowing over a Circular Cylinder," *Journal of Fluid Mechanics,* Vol. **381**, pp. 1-25, 1999.

Neuendorf, R., Lourenco, L., and Wygnanski, I., "On Large Streamwise Structures in a Wall Jet Flowing over a Circular Cylinder," *Physics of Fluids*, Vol. **16**, (7), pp. 2158-2169, 2004.

Newman, B. G., "The Deflection of Plane Jets by Adjacent Boundaries – Coanda Effect," in *Boundary Layer and Flow Control: Its Principles and Applications, Volume 1*, Pergamon Press, edited by G. V. Lachmann, pp. 232-264, 1961.

Radespiel, R., Burnazzi, M., Casper, M., and Scholz, P., "Active flow control for high lift with steady blowing," *The Aeronautical Journal*, Vol. **120** (1223), pp.171-200, 2016.

Vukasinovic, B., DeSalvo, M., Funk, R. and Glezer, A., "Hybrid AFC Actuation: Wind Tunnel Investigations," DARPA CRANE Symposium, April 2021.

Williams, J., Butler, S.F.J. and Wood, M.N., "The aerodynamics of jet flaps," *Aeronautical Research Council*, R&M No. 3304, 1961.